Research Square

Preprints are preliminary reports that have not undergone peer review.
They should not be considered conclusive, used to inform clinical practice,
or referenced by the media as validated information.

# Multiscale Calculation of Equivalent Elastic Modulus for Rock Mass Based on Perturbation Theory

**Lei Wen**

821149277@qq.com

Chongqing Industry Polytechnic College

**Wu Yang**

Chongqing Industry Polytechnic College

**Huayun Yang**

Chongqing Anbiao Testing & Research Institute Co., Ltd.

**Article**

**Keywords:** Engineering rock mass, Equivalent elastic modulus, Multiscale calculation, Initial damage, Perturbation theory

**Posted Date:** July 24th, 2026

**DOI:** https://doi.org/10.21203/rs.3.rs-9881280/v1

**License:** This work is licensed under a Creative Commons Attribution 4.0 International License.
Read Full License

**Additional Declarations:** No competing interests reported.

**Highlights**

1. Established a multiscale calculation approach considering initial damage to obtain the equivalent elastic modulus of a rock mass.
2. The strain tensor caused by meso heterogeneity is regarded as a bridge of macro and microscale for the multiscale perturbation theory.
3. Closer to the laboratory and field test results than the conventional simulation method.
4. Can reflect the macro and micro damage evolution and the equivalent elastic modulus dynamic development of rock mass.

**Multiscale Calculation of Equivalent Elastic Modulus for Rock Mass Based on Perturbation Theory**

Lei Wen[a], Wu Yang[a], Huayun Yang[b]

[a]School of Architectural Engineering, Chongqing Industry Polytechnic University, Chongqing, 401120, China
[b]Chongqing Anbiao Testing & Research Institute Co., Ltd., Chongqing, 400037, China

**Corresponding author**
Lei Wen
Email: 821149277@qq.com
ORCID: 0000-0003-4743-1177

**Abstract**
Elastic modulus is a basic parameter for the safety and stability investigation of rock mass engineering. In this work, we established a multiscale calculation approach considering initial damage to obtain the equivalent elastic modulus of a rock mass. The multiscale calculation results were compared with laboratory test results and validated in the field compression test of grouting solidified bodies. The laboratory rock specimens collected from a deep metal mine in southern China were damaged in a uniaxial compression test. The damaged rock specimens were prepared for laboratory Brazil split tensile and uniaxial compression tests. The research results showed that the compressive stress–strain and tensile load–displacement curves of the damaged rock specimens are in the form of a strictly lower convex function, whereas the field compressive stress–strain curve of the grouting solidified bodies is in the form of a convex function. Considering the initial damage of rock in the laboratory and field tests, the strain tensor caused by meso heterogeneity serves as a bridge of macro and microscale for the multiscale perturbation theory. The multiscale calculation approach could accurately calculate the equivalent elastic modulus of the rock mass. It could also reflect the macro and micro damage evolution and the equivalent elastic modulus dynamic development of the rock mass, and the results are closer to the laboratory and field test results than those of the conventional simulation method. The outcomes of this work can provide a theoretical method reference to solve complex problems in rock engineering.
**Keywords:** Engineering rock mass, Equivalent elastic modulus, Multiscale calculation, Initial damage, Perturbation theory

## Declarations


### Funding

The Science and Technology Research Project of Chongqing Education Commission of China (Grant No. KJQN202003208);

The Doctoral Fund of Chongqing Industry Polytechnic University (Grant No. 2023GZYBSZK1-12);

Chongqing Postdoctoral Science Foundation, China (Grant No. cstc2021jcyj-bshX0032).


### Conflicts of interest/Competing interests

The authors declare that they have no known competing financial interests or personal relationships that could have appeared to influence the work reported in this paper.

### Availability of data and material

The data used to support the findings of this study are available from the corresponding author upon request.

### Code availability

The code used to support the findings of this study are available from the corresponding author upon request.

### Permission for collecting samples from metal mine

The current samples from metal mine are licensed for collection. And those mechanical tests of the sample are used for supporting and mining design of the mine.

### Authors' contributions

1. Lei Wen: Methodology, Investigation, Writing - Original Draft, Writing - Review & Editing, Project administration.
2. : Wu Yang: Writing - Review & Editing, Methodology, Formal analysis.
3. Huayun Yang: Conceptualization, Supervision.

**List of Symbols**

| | |
|---|---|
| $\delta$ | Small parameter of perturbation equation |
| $S_\delta$ | Nonlinear autonomous system |
| $\Gamma_\delta$ | Motion equation of $S_\delta$ |
| $x$ | Displacement coordinate of $S_\delta$ |
| $d$ | Physical dimension parameter of $S_\delta$ |
| $M_n$ | Solution of $\Gamma_\delta$ under the calculation scale $n$, $n$=1, 2, 3… |
| $y$ | Microscale displacement coordinate of $S_\delta$ |
| $T$ | Change cycle of structural variable field |
| $u^\delta$ | Displacement field |
| $\Omega^\delta$ | Micro neighborhood of rock mass |
| $\boldsymbol{\sigma}_{kl}^{\delta}$ | Stress tensor |
| $\boldsymbol{\varepsilon}_{kl}^{\delta}$ | Strain tensor |
| $\boldsymbol{E}_{ijkl}^{\delta}$ | Elasticity tensor |
| $\boldsymbol{S}_{ijkl}^{\delta}$ | Flexible tensor |
| $f_i$ | Volume force |
| $D^\delta$ | Microscale elastic damage factor |
| $\boldsymbol{I}_{mnij}$ | Unit tensor |
| $D_{mnij}^{\delta}$ | Initial elastic damage tensor |
| $\boldsymbol{\chi}_m^{kl}$ | Tensor eigenfunction |
| $\hat{\boldsymbol{\sigma}}_{ij}^{kl}$ | Micro stress tensor characteristic value |
| $\overline{\boldsymbol{E}_{mnkl}^{\delta}}$ | Equivalent elasticity modulus |
| $\overline{\boldsymbol{\sigma}_{ij}^{(0)}}$ | Equivalent stress |
| $\overline{f_i}$ | Equivalent volume force |
| $\overline{u_i}$ | Equivalent displacement |
| $\varsigma$ | Kronecker symbol |
| $D$ | Damage coefficient |
| $Q$ | Load |
| $u$ | Displacement |
| $\sigma_{cs}$ | Uniaxial compressive strength of intact rock |
| $D_t$ | Tensile damage variable |
| $D_{t0}$ | Initial Tensile damage |
| $\overline{\varepsilon}_n^p$ | Equivalent plastic strain occurred in simulation step $n$, $n$= 0, 1, 2… |
| $\varepsilon^p$ | Plastic strain at tensile failure |
| $V_p$ | P-wave velocity of damaged rock specimens |
| $V_{p0}$ | P-wave velocity of intact rock |
| $\Delta D_c$ | Uniaxial compressive damage variable increment |
| $D_{c0}$ | Initial compressive damage |
| $\Delta\overline{E}_c$ | Equivalent elastic modulus increment of simulation step $n$, $n$= 0, 1, 2… |
| $E_c$ | Elastic modulus of intact rock |
| $E_{c0}$ | Initial elastic modulus of damaged rock specimens |
| $\sigma_c$ | Uniaxial compressive stress |
| $\varepsilon_c$ | Uniaxial compressive stain |

## 1 Introduction

Laboratory mechanical test scale is applied to field engineering scale through the reduction method. However, the reduction factor is unreliable. The reduction method cannot reflect the mechanical response process during the rock mass failure (Zhang 2015; Renani 2019; Chen 2021). The laboratory test is employed on intact rocks without considering the impact of macro and microjoints and cracks in the engineering rock mass (Sarfarazi 2016). Field tests are unrepresentative; they can only investigate the surrounding rock characteristics of target areas in a small range (Zhang 2019). Taking the important index for assessing the engineering rock mass characters, elastic modulus, as an example, despite previous research associated with obtaining the elastic modulus (Ashtari 2019; Waqas 2020; Bazulin 2021), there is still a need for a systematic investigation of a new method based on multiscale coupling to calculate the equivalent elastic modulus of a rock mass.

Rock is a typical heterogeneous material. The rock micromechanics theory explains the failure mechanism of a single crack, and it ignores the macroscopic failure of the engineering rock mass. The rock macro-mechanics theory is a phenomenology, which captures the macroscopic characteristics of material failure. However, it does not consider the influence of different scale joints and fissures inside the rock mass. Therefore, there is a need to develop a multiscale calculation approach that can realize the application of the intact rock mechanics parameters to the engineering rock mass (Kim 2012; Wang 2012; Li 2015; Ündül 2015; Hu 2018; Sun 2021). Rock mass failure is the occurrence, development, and penetration of the microcracks, resulting in macrocracks and failure surfaces. To a certain degree, the microscale behavior of the process occurs inside the intact rock, and the macro behavior characterizes the rock mass (Lim 2015; Qu 2016; Nezhad 2016; Zhang 2018; Cao 2019; Hu 2020). Considering a rock with initial damage as a perturbation system, the strain tensor caused by meso heterogeneity can be regarded as a bridge of the macro and microscale to establish the multiscale calculation approach for the rock mass (Radaev 2013; Bacigalupo 2014).

Herein, we established a multiscale calculation approach to investigate the equivalent elastic modulus of a rock mass with initial damage. Brazil split tensile and uniaxial compression tests were conducted to validate the rationality of the new multiscale calculation approach. The damaged rock specimens for laboratory tests were collected from a deep metal mine in southern China and damaged by the uniaxial compression test. The multiscale calculation approach was employed in the field test of the grouting solidified bodies, which was prepared to solve the overall instability of a lead–zinc mine stope.

## 2 Derivation of the Multiscale Calculation Approach

Inside the rock mass are randomly distributed structural planes and caverns, which are heterogeneous. During far-field loading, the microscopic cracks in a rock mass propagate and coalesce to form macroscopic cracks and fracture surfaces, and then the rock mass fails. Assume the standard rock specimen is an ideal model, considering a rock specimen with initial damage as a system, the perturbation theory is an appropriate mathematical method to discuss the movement of the stress and displacement fields of the system (Sanchez-Palencia 1980; Lu 1986).

### *2.1 Fundamental perturbation theory*

If there is a small parameter $\delta$ that is difficult to be accurately determined, and it changes gradually, which can reflect the multiscale expansion process of internal cracks in rock with initial damage. If a rock system $S_\delta$ contains the small parameter $\delta$, the multiscale calculation of the rock mass is a typical perturbation problem. When $\delta = 0$, $S_\delta = S_{\delta 0}$, the perturbation problem is simplified to identify the motion equation $\Gamma_\delta$ of $S_\delta$ by solving the $S_{\delta 0}$. If the motion equation $\Gamma_\delta$ can be reduced to $\Gamma_{\delta 0}$ as a uniformly valid expression, the problem is a regular perturbation problem.

Dimensionless physics equations and boundary conditions of $S_\delta$ to make only one perturbation term with the small parameter $\delta$ appear in the motion equation, the motion equations of the rock mass can be coupled under different scales. The small parameter $\delta$ is the dimensionless perturbation parameter. Therefore, the nondimensionalization of the perturbation problem is also referred to as scaling. The solution of the motion equation $\Gamma_\delta$ of $S_\delta$ is essentially to find the solution of the power series of $\delta$. Therefore, the perturbation method is also called the small parameter expansion method.

For a rock system $S_\delta$ as a nonlinear autonomous system, the secular term is eliminated and independent variables of multiple geometric dimension scales are introduced to make the series solution of $S_\delta$ uniformly converge. The general solving procedure of the fundamental perturbation theory (Truhar 2021) is depicted in Eq. (1) ~ Eq. (10) (Fig. 1). Fig. 1 introduces a physical dimension parameter $d$. As shown in Fig. 1, $M_n$ is the solution of the motion equation $\Gamma_\delta$ under the physical dimension calculation scale $n$, $n = 1, 2, 3\ldots$

### *2.2 Asymptotic expansion of strain tensor*

It is assumed that the internal microstructure of a rock mass is distributed periodically. During external loading, stress is concentrated in a neighborhood around the micro-damaged structure inside the rock mass. The structural variable field at point $x$ rapidly changes periodically within a microscale neighborhood $\delta$. The macroscale variable can be regarded as a constant (variable separation), and the multiscale description (Fig. 2) of the rock mass is as

follows:

$$\Phi^{\delta}(x)=\Phi(x,y) \tag{11}$$

$$y=x/\delta \quad (0<\delta<1) \tag{12}$$

$$\Phi(x,y)=\Phi(x,y+T) \tag{13}$$

The partial derivative of displacement coordinate $x$ is defined as follows:

$$\nabla\rightarrow\nabla_x+\frac{1}{\delta}\nabla_y \tag{14}$$

$$\nabla u^{\delta}(x)=\nabla_x u(x,y)\big|_{y=\frac{x}{\delta}}+\frac{1}{\delta}\nabla_y u(x,y)\big|_{y=\frac{x}{\delta}} \tag{15}$$

where $u^{\delta}(x)$ is the displacement field, $u^{\delta}(x)=u(x,y)=u(x,x/\delta)$.

According to Fig 1, the asymptotic expansion of $u^{\delta}(x)$ is expressed as follows:

$$u^{\delta}(x,x/\delta)=u^{(0)}(x,y)+\delta u^{(1)}(x,y)+\delta^2u^{(2)}(x,y)+\mathrm{L}\ +\delta^n u^{(n)}(x,y),y=\frac{x}{\delta} \tag{16}$$

where ($n$) is the number of the scale, the larger the $n$, the smaller the scale of the physical dimension.
According to the continuum mechanics theory (Voyiadjis 2021; Radaev 2013; Bacigalupo 2014), the strain tensor $\boldsymbol{\varepsilon}_{kl}^{\delta}$ is rewritten as follows:

$$\boldsymbol{\varepsilon}_{kl}^{\delta}=\frac{1}{2}\left(\frac{\partial \boldsymbol{u}_k^{\delta}}{\partial \boldsymbol{x}_l^{\delta}}+\frac{\partial \boldsymbol{u}_l^{\delta}}{\partial \boldsymbol{x}_k^{\delta}}\right)+\frac{1}{2}\frac{\partial \boldsymbol{u}_k^{\delta}}{\partial \boldsymbol{x}_l^{\delta}}\frac{\partial \boldsymbol{u}_l^{\delta}}{\partial \boldsymbol{x}_k^{\delta}} \tag{17}$$

The higher-order term in Eq. (17) can be omitted due to the small deformation, and it can be expressed as follows:

$$\boldsymbol{\varepsilon}_{kl}^{\delta}=\frac{1}{2}\left(\frac{\partial \boldsymbol{u}_k^{\delta}}{\partial \boldsymbol{x}_l^{\delta}}+\frac{\partial \boldsymbol{u}_l^{\delta}}{\partial \boldsymbol{x}_k^{\delta}}\right) \tag{18}$$

Substituting Eq. (16) into Eq. (18), we obtain

$$\begin{aligned}\boldsymbol{\varepsilon}_{kl}^{\delta}=&\frac{1}{2}\frac{1}{\delta}\left(\frac{\partial \boldsymbol{u}_k^{(0)}}{\partial x_l}+\frac{\partial \boldsymbol{u}_l^{(0)}}{\partial \boldsymbol{y}_k}\right)+\frac{1}{2}\left(\frac{\partial \boldsymbol{u}_k^{(0)}}{\partial \boldsymbol{x}_l}+\frac{\partial \boldsymbol{u}_l^{(0)}}{\partial \boldsymbol{x}_k}+\frac{\partial \boldsymbol{u}_k^{(1)}}{\partial \boldsymbol{y}_l}+\frac{\partial \boldsymbol{u}_l^{(1)}}{\partial \boldsymbol{y}_k}\right)+\frac{1}{2}\delta\left(\frac{\partial \boldsymbol{u}_k^{(1)}}{\partial \boldsymbol{x}_l}+\frac{\partial \boldsymbol{u}_l^{(1)}}{\partial \boldsymbol{x}_k}+\frac{\partial \boldsymbol{u}_k^{(2)}}{\partial \boldsymbol{y}_l}+\frac{\partial \boldsymbol{u}_l^{(2)}}{\partial \boldsymbol{y}_k}\right)\\&+\frac{1}{2}\delta^2\left(\frac{\partial \boldsymbol{u}_k^{(2)}}{\partial \boldsymbol{x}_l}+\frac{\partial \boldsymbol{u}_l^{(2)}}{\partial \boldsymbol{x}_k}+\frac{\partial \boldsymbol{u}_k^{(3)}}{\partial \boldsymbol{y}_l}+\frac{\partial \boldsymbol{u}_l^{(3)}}{\partial \boldsymbol{y}_k}\right)+\mathrm{L}\ +\frac{1}{2}\delta^{n-1}\left(\frac{\partial \boldsymbol{u}_k^{(n-1)}}{\partial \boldsymbol{x}_l}+\frac{\partial \boldsymbol{u}_l^{(n-1)}}{\partial \boldsymbol{x}_k}+\frac{\partial \boldsymbol{u}_k^{(n)}}{\partial \boldsymbol{y}_l}+\frac{\partial \boldsymbol{u}_l^{(n)}}{\partial \boldsymbol{y}_k}\right)\end{aligned} \tag{19}$$

The asymptotic expansion of $\boldsymbol{\varepsilon}_{kl}^{\delta}$ is as follows:

$$\boldsymbol{\varepsilon}_{kl}^{\delta}=\frac{1}{\delta}\boldsymbol{\varepsilon}_{kl}^{(-1)}(x,y)+\boldsymbol{\varepsilon}_{kl}^{(0)}(x,y)+\delta\boldsymbol{\varepsilon}_{kl}^{(1)}(x,y)+\delta^2\boldsymbol{\varepsilon}_{kl}^{(2)}(x,y)+\mathrm{L}\ +\delta^{n-1}\boldsymbol{\varepsilon}_{kl}^{(n-1)}(x,y) \tag{20}$$

where $\varepsilon_{kl}^{(-1)}(x,y)$ means that there is only a strain tensor without considering the meso heterogeneity under the (-1) scale. In $\boldsymbol{\varepsilon}_{kl}^{(0)}(x,y)=\frac{1}{2}\left(\frac{\partial \boldsymbol{u}_k^{0}}{\partial \boldsymbol{x}_l}+\frac{\partial \boldsymbol{u}_l^{0}}{\partial \boldsymbol{x}_k}+\frac{\partial \boldsymbol{u}_k^{1}}{\partial \boldsymbol{y}_l}+\frac{\partial \boldsymbol{u}_l^{1}}{\partial \boldsymbol{y}_k}\right)$, $\frac{1}{2}\left(\frac{\partial \boldsymbol{u}_k^{1}}{\partial \boldsymbol{y}_l}+\frac{\partial \boldsymbol{u}_l^{1}}{\partial \boldsymbol{y}_k}\right)$ is the strain tensor caused by meso heterogeneity under the (0) scale.

### *2.3 Governing equations*

Based on the equivalent stress hypotheses (Zhang 2020), in the microneighborhood $\Omega^{\delta}$ of a rock mass, the elasticity tensor $\boldsymbol{E}_{ijkl}^{\delta}$ and the flexible tensor $\boldsymbol{S}_{ijkl}^{\delta}$ can be expressed as a function with the microscale displacement as follows:

$$\begin{aligned}&\boldsymbol{E}_{ijkl}^{\delta}(x)=\boldsymbol{E}_{ijkl}^{\delta}(x,y) \quad (a)\\&\boldsymbol{S}_{ijkl}^{\delta}(x)=\boldsymbol{S}_{ijkl}^{\delta}(x,y) \quad (b)\end{aligned} \tag{21}$$

where $\boldsymbol{E}_{ijkl}^{\delta}$ is the inverse of $\boldsymbol{S}_{ijkl}^{\delta}$.

The equilibrium differential equation is described as follows:

$$\boldsymbol{\sigma}_{ij,j}^{\delta} = -f_i \tag{22}$$

where $\boldsymbol{\sigma}_{ij}^{\delta}$ is the stress, and $f_i$ is the volume force.

Therefore, the constitutive equation coupled with the microelastic damage factor $D^{\delta}$ (Lemaitre 1985) is expressed as follows:

$$\boldsymbol{\sigma}_{ij}^{\delta} = \left(1 - D^{\delta}\right) \boldsymbol{E}_{ijkl}^{\delta} \boldsymbol{\varepsilon}_{kl}^{\delta} \tag{23}$$

Substituting Eq. (20) into Eq. (23), the asymptotic expansion of the stress tensor $\boldsymbol{\sigma}_{ij}^{\delta}$ can be derived as

$$\begin{aligned} &\boldsymbol{\sigma}_{ij}^{\delta} = \frac{1}{\delta}\boldsymbol{\sigma}_{ij}^{(-1)}(x,y) + \boldsymbol{\sigma}_{ij}^{(0)}(x,y) + \delta\boldsymbol{\sigma}_{ij}^{(1)}(x,y) + \delta^2\boldsymbol{\sigma}_{ij}^{(2)}(x,y) + \mathrm{L} + \delta^{n-1}\boldsymbol{\sigma}_{ij}^{(n-1)}(x,y), \\ &\boldsymbol{\sigma}_{ij}^{\delta}(x,y) = \left(1 - D^{\delta}\right)\boldsymbol{E}_{ijkl}^{\delta}\boldsymbol{\varepsilon}_{kl}^{\delta}(x,y) \end{aligned} \tag{24}$$

Considering the initial damage, $\boldsymbol{E}_{ijkl}^{\delta}$ can be rewritten as follows:

$$\boldsymbol{E}_{mnkl}^{\delta} = \left(\boldsymbol{I}_{mnij} - D_{mnij}\right)\boldsymbol{E}_{ijkl}^{\delta} = \left(\boldsymbol{I}_{mnij} - D_{mnij}\right)\boldsymbol{E}_{ijkl}(x/\delta) = \left(\boldsymbol{I}_{mnij} - D_{mnij}\right)\boldsymbol{E}_{ijkl}(y) \tag{25}$$

where $\boldsymbol{I}_{mnij}$ is the unit tensor, and $D_{mnij}$ is the initial elastic damage tensor. The $D_{mnij}$ takes a symmetric tensor. Assume that the tensor components of $D_{mnij}$ in each principal direction are equal.

Substituting Eq. (25) into Eq. (24), we obtain the following:

$$\boldsymbol{\sigma}_{mn}^{(-1)} = \boldsymbol{E}_{mnkl}^{\delta}\boldsymbol{\varepsilon}_{kl}^{(-1)} \tag{26}$$

$$\boldsymbol{\sigma}_{mn}^{(0)} = \boldsymbol{E}_{mnkl}^{\delta}\boldsymbol{\varepsilon}_{kl}^{(0)} - \boldsymbol{E}_{mnkl}^{\delta}\boldsymbol{\varepsilon}_{kl}^{(1)} \tag{27}$$

$$\boldsymbol{\sigma}_{mn}^{(1)} = \boldsymbol{E}_{mnkl}^{\delta}\boldsymbol{\varepsilon}_{kl}^{(1)} - \boldsymbol{E}_{mnkl}^{\delta}\boldsymbol{\varepsilon}_{kl}^{(2)} \tag{28}$$

Substituting Eq. (24) into Eq. (22), we obtain the following:

$$\begin{aligned} &\frac{1}{\delta}\left[\frac{\partial\boldsymbol{\sigma}_{mn}^{(-1)}(x,y)}{\partial\boldsymbol{x}_n} + \frac{1}{\delta}\frac{\partial\boldsymbol{\sigma}_{mn}^{(-1)}(x,y)}{\partial\boldsymbol{y}_n}\right] + \left[\frac{\partial\boldsymbol{\sigma}_{mn}^{(0)}(x,y)}{\partial\boldsymbol{x}_n} + \frac{1}{\delta}\frac{\partial\boldsymbol{\sigma}_{mn}^{(0)}(x,y)}{\partial\boldsymbol{y}_n}\right] + \\ &\delta\left[\frac{\partial\boldsymbol{\sigma}_{mn}^{(1)}(x,y)}{\partial\boldsymbol{x}_n} + \frac{1}{\delta}\frac{\partial\boldsymbol{\sigma}_{mn}^{(1)}(x,y)}{\partial\boldsymbol{y}_n}\right] + \delta^2\left[\frac{\partial\boldsymbol{\sigma}_{mn}^{(2)}(x,y)}{\partial\boldsymbol{x}_n} + \frac{1}{\delta}\frac{\partial\boldsymbol{\sigma}_{mn}^{(2)}(x,y)}{\partial\boldsymbol{y}_n}\right] + \mathrm{L} + f_m = 0 \end{aligned} \tag{29}$$

Fixing the coefficient of each item, including $\delta$, as 0, the balance control equations of every order are obtained as follows:

$$\begin{aligned} &O\left(\delta^{-2}\right): \quad \frac{\partial\boldsymbol{\sigma}_{mn}^{(-1)}(x,y)}{\partial\boldsymbol{y}_n} = 0 \\ &O\left(\delta^{-1}\right): \quad \frac{\partial\boldsymbol{\sigma}_{mn}^{(-1)}(x,y)}{\partial\boldsymbol{y}_n} + \frac{\partial\boldsymbol{\sigma}_{mn}^{(0)}(x,y)}{\partial\boldsymbol{y}_n} = 0 \\ &O\left(\delta^{0}\right): \quad \frac{\partial\boldsymbol{\sigma}_{mn}^{(0)}(x,y)}{\partial\boldsymbol{y}_n} + \frac{\partial\boldsymbol{\sigma}_{\eta\kappa}^{(1)}(x,y)}{\partial\boldsymbol{y}_n} + f_m = 0 \\ &O\left(\delta^{1}\right): \quad \frac{\partial\boldsymbol{\sigma}_{mn}^{(1)}(x,y)}{\partial\boldsymbol{y}_n} + \frac{\partial\boldsymbol{\sigma}_{mn}^{(2)}(x,y)}{\partial\boldsymbol{y}_n} = 0 \\ &\mathrm{M} \\ &O\left(\delta^{n}\right): \quad \frac{\partial\boldsymbol{\sigma}_{mn}^{(n)}(x,y)}{\partial\boldsymbol{y}_n} + \frac{\partial\boldsymbol{\sigma}_{mn}^{(n+1)}(x,y)}{\partial\boldsymbol{y}_n} = 0, \qquad n = 1,2,3\ldots \end{aligned} \tag{30}$$

Substituting Eq. (26), Eq. (27), and Eq. (28) into Eq. (30), we obtain the following:

$$\frac{\partial}{\partial \boldsymbol{y}_j}\left(\boldsymbol{E}^{\delta}_{mnkl}\frac{\partial \boldsymbol{u}^{(0)}_k}{\partial \boldsymbol{y}_l}\right)=0 \tag{31}$$

Based on the periodicity of the microunit, $u^{(0)}(x,y)=u^{(0)}(x)$, then $\boldsymbol{\sigma}^{(-1)}_{mn}=0$. The $u^{(0)}$ represents the homogenized displacement field of the macrostructure.

$$\frac{\partial \boldsymbol{\sigma}^{(0)}_{mn}(x,y)}{\partial \boldsymbol{y}_n}=\frac{\partial}{\partial \boldsymbol{y}_n}\left[\boldsymbol{E}^{\delta}_{mnkl}\left(\frac{\partial \boldsymbol{u}^{(0)}_k}{\partial \boldsymbol{x}_l}+\frac{\partial \boldsymbol{u}^{(1)}_k}{\partial \boldsymbol{y}_l}\right)\right]=0 \tag{32}$$

Considering that $u^{(1)}$ conforms to a periodicity, Eq. (32) is transformed as follows:

$$\begin{cases}\boldsymbol{\sigma}^{(0)}_{mn}=\hat{\boldsymbol{\sigma}}^{kl}_{mn}(y)\dfrac{\partial \boldsymbol{u}^{(0)}_k}{\partial \boldsymbol{x}_l}\\ \boldsymbol{u}^{(1)}_m=-\boldsymbol{\chi}(y)^{kl}_m\dfrac{\partial \boldsymbol{u}^{(0)}_k}{\partial \boldsymbol{x}_l}\end{cases} \tag{33}$$

where $\hat{\boldsymbol{\sigma}}^{kl}_{mn}$ is the microstress tensor characteristic. $\boldsymbol{\chi}^{kl}_m$ represents a tensor eigenfunction.

The governing equation of $\boldsymbol{\chi}^{kl}_m$ is represented as follows:

$$\frac{\partial}{\partial \boldsymbol{y}_n}\left\{\boldsymbol{E}^{\delta}_{mnkl}\left[\left(\varsigma_{mk}\varsigma_{nl}+\varsigma_{ml}\varsigma_{nk}\right)+\frac{\partial \boldsymbol{\chi}^{kl}_m}{\partial \boldsymbol{y}_n}\right]\right\}=0 \tag{34}$$

where $\varsigma$ is the Kronecker symbol.

To characterize the microdisplacement, the virtual displacement is introduced to solve the tensor eigenfunction by the finite element method based on the variational principle (Qin 2006).

The microequilibrium equation is obtained based on the expansion of boundary conditions and the Gauss integral theorem as follows:

$$\frac{\partial \hat{\boldsymbol{\sigma}}^{kl}_{mn}(y)}{\partial \boldsymbol{y}_n}=0 \tag{35}$$

Therefore, the microconstitutive equation is formulated as follows:

$$\hat{\boldsymbol{\sigma}}^{kl}_{mn}(y)=\boldsymbol{E}^{\delta}_{mnkl}\left[\frac{1}{2}\left(\varsigma_{mk}\varsigma_{nl}+\varsigma_{ml}\varsigma_{nk}\right)+\frac{\partial \boldsymbol{\chi}^{kl}_m}{\partial \boldsymbol{y}_n}\right]\frac{\partial \boldsymbol{u}^{(0)}_k}{\partial \boldsymbol{x}_l} \tag{36}$$

The homogenized macro equivalent elasticity modulus $\overline{\boldsymbol{E}^{\delta}_{mnkl}}$ considering the initial damage can be expressed as follows:

$$\overline{\boldsymbol{E}^{\delta}_{mnkl}}=\frac{1}{T}\int_T \boldsymbol{E}^{\delta}_{mnkl}\left[\frac{1}{2}\left(\varsigma_{mk}\varsigma_{nl}+\varsigma_{ml}\varsigma_{nk}\right)+\frac{\partial \boldsymbol{\chi}^{kl}_m}{\partial \boldsymbol{y}_n}\right]dT \tag{37}$$

Then, substituting Eq. (37), Eq. (27), and Eq. (28) into Eq. (30), $\overline{\boldsymbol{\sigma}^{(0)}_{mn}}$ is the equivalent stress and is expressed as follows:

$$\overline{\boldsymbol{\sigma}^{(0)}_{mn}}=\overline{\boldsymbol{E}^{\delta}_{mnkl}}\frac{\partial \boldsymbol{u}^{(0)}_k}{\partial \boldsymbol{x}_l} \tag{38}$$

Considering only two scales, the multiscale equivalent elastic governing equation within the neighborhood $\Omega^{\delta}$ of the rock mass is expressed as follows:

$$\begin{cases} \overline{\boldsymbol{\sigma}_{mn,n}^{(0)}} = -\overline{f_m} \\ \overline{\boldsymbol{\sigma}_{mn}^{(0)}}\boldsymbol{n}_n = t_m \\ u_m^{(0)} = \overline{u_m} \end{cases} \tag{39}$$

where $\overline{f_m}$ is the equivalent volume force, $\overline{f_m} = \frac{1}{T}\int_T f_m dT$. $t_m$ is the boundary surface force, $\boldsymbol{n}_n$ the Normal vector of the boundary surface force, and $\overline{u_m}$ the equivalent displacement.

## 3 Implementation and Validation

### *3.1 Solution procedure*

The multiscale calculation approach for the equivalent elastic modulus of a rock mass is shown in Fig. 3.

In Fig. 3, the internal variable of iterative calculation is the damage coefficient, $D$. The load $Q$ and displacement $u$ of each load calculation step are updated. The equivalent mechanical parameters of each updated damage state can be obtained.

The multiscale calculation approach can reflect the macro and microdamage evolution and equivalent elastic modulus development during the rock mass failure.

The multiscale calculation approach for the equivalent elastic modulus of the rock mass was programmed using MATLAB. The finite element numerical model was established using COMSOL to calculate the mechanics response behavior of rock specimens under different test conditions. Figure 4 shows a flowchart of the numerical simulation.

### *3.2 Materials and test procedure*

Rock specimens with initial damage of typical limestone were collected from a deep metal mine in southern China (Fig. 5). The initial damage is caused by different uniaxial compressive stresses ($0.25\sigma_{cs}$, $0.4\sigma_{cs}$, $0.5\sigma_{cs}$, $0.65\sigma_{cs}$, $0.75\sigma_{cs}$; $\sigma_{cs}$ is the uniaxial compressive strength of intact rock) (Eberhardt 1999). Specimens with different initial damage were prepared for several Brazil splitting tests ($\varphi$50 × 50 mm) and uniaxial compression test ($\varphi$50 × 100 mm), which were performed using an INSTRON Electro-hydraulic servo universal testing machine (Fig. 6).

The P-wave velocity of the damaged rock specimens $V_p$ is shown in Fig. 7, which was obtained using the RSM-SY5 (T) nonmetallic acoustic wave detector (Fig. 8).

Figure 7 shows that $V_p$ decreases as the initial damage increases. P-wave velocity can characterize the degree of damage of rock specimens. A similar result is reported in Xia (2013).

Figure 9 shows the Computed Tomography (CT) scan results of the damaged rock specimens, which were obtained using the AX-3000 industrial micro CT scan system (Fig. 10).

As shown in Fig. 9, the higher the initial damage, the more the white areas on the CT scan section of rock specimens and the more the pores and cracks.

The test procedure is shown in Fig. 11.

### *3.3 Case I: Brazil split tensile test simulation*

The material property was investigated using a damage plasticity model. The grid is divided as shown in Fig. 12. The strength attribute only considers the Brazilian split tensile strength, which is defined by the product of the Brazilian split tensile strength of intact rock and the cumulative damage coefficient. The density was set to a constant when the basic plasticity was assigned. The elastic modulus and Poisson's ratio were calculated in real-time using MATLAB. The macro (in a localized way) and micro (through progressive homogenization) model parameter information exchanged in double directions.

It is not suitable to define the damage variable by the elastic modulus during the Brazil split tensile process (Li 2017). Therefore, Case I only explores the adaptability of the multiscale calculation approach in rock tensile-failure simulation.

The tensile deformation of cracks is regarded as plastic deformation. The tensile damage variable ($D_t$) is defined as follows (Martini 1997):

$$D_t = \frac{\overline{\varepsilon}_n^p}{\varepsilon^p} + D_{t0}, \tag{40}$$

where $\overline{\varepsilon}_n^p$ is the equivalent plastic strain in the simulation step $n$, $n$ = 0, 1, 2, … When $n$ = 0, $\varepsilon_n^p = 0 \cdot \varepsilon^p$ is the plastic strain at the tensile failure. $D_{t0}$ is the initial tensile damage of the rock specimens.

The $D_{t0}$ of the multiscale simulation and the conventional finite element simulation is rewritten as follows (Xia 2013):

$$D_{t0}=1-\frac{V_p^2}{V_{p0}^2} \quad (41)$$

where $V_{p0}$ is the P-wave velocity of intact rock.

The damaged rock specimens and the corresponding numerical models of the Brazilian split tensile test are shown in Fig. 13.

In Fig. 13, the high-brightness blue area indicates the damage on the rock specimens. Under the homogenized expression, the initial damage is randomly distributed in the rock specimens. The damage distribution of the numerical models in Fig. 12 is similar to the typical CT scan section of the rock specimens in Fig. 9.

The typical split failure specimen after the Brazil split tensile test and the numerical model calculation result is shown in Fig. 14.

In Fig. 14, the darker the blue area in the numerical models, the greater the displacement of the rock specimen. The failure form f the rock sample in the numerical model is consistent with that of the Brazil split tensile test, indicating that the simulation calculation results are reliable.

The Brazil split tensile load–displacement curves of rock specimens with different initial damage are shown in Fig. 15. The figure compares the multiscale calculation, conventional finite element simulation, and test results.

Figure 15 shows the following:

(1) The load–displacement curves of the Brazil split tensile test are in the form of an obvious strictly lower convex function.

(2) The multiscale calculation results are closer to the test results than those of the conventional finite element simulation, although the peak tensile stresses for the three methods are similar.

(3) Only the load–displacement curves obtained using the multiscale calculation approach are consistent with those of the Brazil test. The multiscale calculation approach is more suitable to assess the mechanical response process of a rock mass than the conventional finite element simulation.

### *3.4 Case 2: Uniaxial compression test simulation*

The strength attribute only considers the uniaxial compressive strength, which is defined by the product of the uniaxial compressive strength of intact rock and the cumulative damage coefficient. Both ends of the specimen model were loaded at a loading rate of 0.001 mm/step. The damaged rock specimens and the corresponding numerical models for uniaxial compression tests are shown in Fig. 16.

The increase in the uniaxial compressive damage ($\Delta D_c$) is defined as follows (Lemaitre 1985):

$$\Delta D_c = \frac{\Delta \bar{E}_c}{E_c}, \quad (42)$$

where $\Delta \bar{E}_c$ is the increase in the equivalent elastic modulus of the simulation step $n$, $n$ = 0, 1, 2, … When $n$ = 0, $\Delta \bar{E}_c = 0$. $E_c$ is the elastic modulus of intact rock.

$$D_{c0} = 1 - \frac{E_{c0}}{E_c}, \quad (43)$$

where $D_{c0}$ is the initial compressive damage of the rock specimens and $E_{c0}$ is the initial elastic modulus of the damaged rock specimens.

If the multiscale calculation model converges at the $m$-th step, $\bar{E}_{cm}$ is the equivalent elastic modulus of the rock specimen with initial damage, $D_{c0}$.

Figure 17 shows the uniaxial compressive stress-strain curves of the rock specimens with different initial damage. The multiscale calculation results agree well with those of the conventional finite element simulation and Brazil test. We examined the damage evolution results.

From Fig. 17, we obtain the following:

(1) The damage on the rock specimens gradually increased at the initial stage, and then rapidly and remained stable to the end.

(2) The stress-strain curves of the uniaxial compression test are in the form of a monotonically increasing concave function.

(3) Based on the same peak uniaxial compressive stress, the multiscale calculation results are closer to the test results.

(3) The variation of strain in the test results is greater than that of the simulation calculation results. The reason is that the development of numerical models is still relatively ideal, although the multiscale calculation approach was as close as possible to the true state of the damage evolution of the rock mass.

The multiscale calculation results of the equivalent elastic modulus for the rock specimens with initial damage are listed in Table 1.

Table 1 shows that The equivalent elastic modulus of the multiscale calculation approach is closer to the laboratory test results, indicating that the results of the multiscale calculation approach are relatively accurate and reasonable. The damage can be regarded as a bridge of macro and microscale for the multiscale calculation approach to identify the equivalent elastic modulus of the rock mass.

## 4 Applications and Discussion

### *4.1 Project background*

The overall instability of 0# stope in the middle of Sh-320 m of a lead–zinc mine caused a large area of collapse (Fig. 18). The solution-adopted field is the grouting reinforcement.

A downward segmented grouting method is adopted in the collapsed area. The grouting material is pure cement slurry. Figure 19 shows the effects of the grouting reinforcement. The grouting solidified bodies is regarded as a rock mass with irregular joint fissures. A broken ore or rock is the aggregate of the solidified body. The contact surface between the rock and cement slurry can be analogous to the original joint surface or fractured structural plane. Therefore, the compressive strength and elastic modulus of intact rock can be used as the initial parameters to obtain the equivalent elastic modulus according to the multiscale calculation approach.

### *4.2 Multiscale Calculation results*

The uniaxial compressive stress–strain curve of the grouting solidified bodies is obtained by the field compression test, which is compared with the multiscale calculation results (Fig. 20).

Figure 20 shows that the multiscale calculation approach obtained accurate stress–strain curves of the grouting solidified bodies before the field peak uniaxial compressive stress.

The multiscale calculation results of equivalent elastic modulus for the grouting solidified bodies are lsited in Table 2.

Table 2 shows that the multiscale calculation approach obtained accurate equivalent elastic modulus of the grouting solidified bodies with the rock as aggregate.

Figure 20 and Table 2 show that the multiscale calculation approach can be employed in assessing the elastic modulus of a rock sample in the engineering field.

### *4.3 Discussion*

Multiscale analysis is a method for investigating the macroproperties through the microstructure information of multiphase composite materials. It is based on asymptotic homogenization (Weinan 2007). Considering the initial damage of rock, the perturbation theory multiscale calculation approach can obtain accurate equivalent elastic modulus of a rock mass. Similarly, if a suitable bridge of macro and microscale is identified, the multiscale calculation approach can also be used to determine parameters of the mechanical properties of other heterogeneous materials. Thus, the parameters of other mechanical properties of a rock mass can be obtained using the equivalent elastic modulus and the multiscale calculation approach.

However, the post-peak stress–strain curves of the grouting solidified bodies obtained using the multiscale calculation approach are different from the real field test results (Fig. 21). The post-peak stress-strain characteristics of rock have a strong uncertainty, there is a possibility that can be attributed to the is strain-softening behavior after the failure of the grouting solidified bodies, which is different from that of deep brittle rock (Doitrand 2021). The multiscale calculation approach proposed herein does not introduce the strain-softening parameter; thus, it cannot accurately access the complete mechanical behavior of the grouting solidified bodies.

Nonetheless, the results of the multiscale calculation model before the peak stress are accurate, which is established based on a coupling condition of the strain caused by the meso heterogeneity of rock under the macroscale. On the one hand, we considered the initial damage of rock, which is consistent with the actual state of rock. On the other hand, the elastic modulus depends on the stress level of rock. However, the conventional damage model of rock regards the elastic modulus as a constant. But the solution process of the multiscale calculation method considers an dynamic change of the elastic modulus of rock during the loading. Suitable multiscale calculation models for the rock masses with different properties will be investigated in our future studies.

## 5 Conclusions

Herein, we propose a multiscale approach for calculating the equivalent elastic modulus of rock masses considering the initial damage. The approach considers the macro and microproperties of rock and rock masses. From the obtained results, we draw the following conclusions:

(1) The multiscale calculation approach can be employed in the engineering field to calculate the elastic modulus

of rock masses. It can reflect the macro and microdamage evolution and equivalent elastic modulus development of rock masses with initial damage.

(2) The P-wave velocity of damaged rock decreases with an increase in initial damage, which can characterize the damage degree of rocks. The uniaxial compressive damage increases gradually in the initial stage, rapidly develops, and remains stable.

(3) The load–displacement curves of the Brazil split tensile test and the stress–strain curves of the uniaxial compression test show a strictly lower convex function, whereas the compressive stress–strain curve shows a convex function in the on-site test for grouting solidified bodies.

(4) The multiscale calculation results are closer to the test results than those of the conventional simulation, however, the curves are consistent with those of the test. Considering the initial damage, the equivalent elastic modulus obtained using the multiscale calculation approach is similar to both the laboratory and field test results.

**Acknowledgements**

The authors are grateful to the science and technology research project of Chongqing Education Commission of China (Grant No. KJQN202003208), for supporting this research. This study is also supported by the Doctoral Fund of Chongqing Industry Polytechnic University (Grant No. 2023GZYBSZK1-12) and Chongqing Postdoctoral Science Foundation (Grant No. cstc2021jcyj-bshX0032).

**References**


Ashtari M, Mousavi SE, Cheshomi A, Khamechian M (2019) Evaluation of the single compressive strength test in estimating uniaxial compressive and Brazilian tensile strengths and elastic modulus of marlstone. Eng Geol 248: 256–266. https://doi.org/10.1016/j.enggeo.2018.12.005

Bacigalupo A (2014) Second-order homogenization of periodic materials based on asymptotic approximation of the strain energy: formulation and validity limits. Meccanica 49: 1407–1425. https://doi.org/10.1007/s11012-014-9906-0

Bazulin M, Sabitov D, Charara M (2021) Determination of the elastic parameters of a VTI medium from sonic logging data using deep learning. Comput Geosci (12): 104759. https://doi.org/10.1016/j.cageo.2021.104759

Cao RH, et al. (2019) Crack initiation, propagation, and failure characteristics of jointed rock or rock-like specimens: A review. Adv Civ Eng 2019: 6975751. https://doi.org/10.1155/2019/6975751

Chen GQ, Li H, Wei T, Zhu J (2021) Searching for multistage sliding surfaces based on the discontinuous dynamic strength reduction method. Eng Geol 286(4): 106086. https://doi.org/10.1016/j.enggeo.2021

Doitrand A, Cornetti P, Sapora A, Estevez R (2021) Experimental and theoretical characterization of mixed mode brittle failure from square holes. Int J Fract 228(1): 33–43. https://doi.org/10.1007/s10704-020-00512-9

Eberhardt E, Stead D, Stimpson B (1999) Quantifying progressive pre-peak brittle fracture damage in rock during uniaxial compression. Int J Rock Mech Min Sci 36(3): 361–380. https://doi.org/10.1016/S0148-9062(99)00019-4

Hu K, Zhu QZ, Chen L Shao JF, Liu J (2018) A micromechanics-based elastoplastic damage model for rocks with a brittle–ductile transition in mechanical response. Rock Mech Rock Eng 51: 1729–1737. https://doi.org/10.1007/s00603-018-1427-z

Hu JH, et al. (2020) Mechanical properties and crack evolution of double-layer composite rock-like specimens with two parallel fissures under uniaxial compression. Theor. Appl. Fract. Mech 108: 102610. https://doi.org/10.1016/j.tafmec.2020.102610

Kim H, Cho JW, Song I, Min KB (2012) Anisotropy of elastic moduli, P-wave velocities, and thermal conductivities of Asan Gneiss, Boryeong Shale, and Yeoncheon Schist in Korea. Eng Geol 147–148: 68–77. https://doi.org/10.1016/j.enggeo.2012.07.015

Lemaitre J (1985) Coupled elasto-plasticity and damage constitutive equations. Comput Methods Appl Mech Eng 51(1–3): 31–49. https://doi.org/10.1016/0045-7825(85)90026-X

Lu ZQ (1986) JKM perturbation theory, relaxation perturbation theory, and their applications to inverse scattering: theory and reconstruction algorithms. IEEE T Ultrason Ferr 33(6): 722–730. https://doi.org/10.1109/T-UFFC.1986.26888

Lim KW, et al. (2015) Multiscale characterization and modeling of granular materials through a computational mechanics avatar: a case study with experiment. Acta Geotech 11(2): 1–11. https://doi.org/10.1007/s11440-015-0405-9

Li L, Larsen I. Holt RM (2015) Laboratory observation and micromechanics-based modelling of sandstone on different scales. Rock Mech Rock Eng 48: 1407–1422. https://doi.org/10.1007/s00603-014-0642-5

Li ZX, Sun ZH, Guo L, Chen HT, Yu Y (2007) Concurrent multiscale modeling of structures and damage analysis. Chin J Southeast Univ (Nat Sci Ed) 37(2): 251–260. https://doi.org/10.3321/j.issn:1001-0505.2007.02.014

Martini CD, Read RS, Martino JB (1997) Observations of brittle failure around a circular test tunnel. Int J Rock Mech Min Sci 34(7): 1065–1073. https://doi.org/10.1016/S1365-1609(97)90200-8

Nezhad MM, Zhu, HH, Ju, JW (2016) A simplified multiscale damage model for the transversely isotropic shale rocks under tensile loading. Int J Damage Mech 25(5): 705–726. https://doi.org/10.1177/1056789516639531

Qu MM, Jiang DZ, Lu LX (2016) An optimal scheme for numerical evaluation of Eshelby tensors and its implementation in a MATLAB package for simulating the motion of viscous ellipsoids in slow flows. Comput Geosci 96: 98–108. https://doi.org/10.1016/j.cageo.2016.08.005

Qin QH, Yang QS (2006) Macro-micro theory on multi-field coupling behavior of heterogeneous materials. Springer, Beijing, Higher Education Press.

Radaev YN (2013) Asymptotic axes of stress tensors and strain increment tensors in mechanics of compressible continua. Mech. Solids 48(5): 546–552. https://doi.org/10.3103/S0025654413050105

Renani HR, Martin CD, Varona P, Lorig L (2019) Stability analysis of slopes with spatially variable strength properties. Rock Mech Rock Eng 52: 3791–3808. https://doi.org/10.1007/s00603-019-01828-2

Sanchez-Palencia E (1980) Non-Homogeneous Media and Vibration Theory. Lect Notes Phys 127. https://doi.org/10.1007/3-540-10000-8

Sarfarazi V, Haeri H (2016) A review of experimental and numerical investigations about crack propagation. Comput Concr 18(2): 235–266. https://doi.org/10.12989/cac.2016.18.2.235

Sun W, Wu SC, Xu XL (2021) Mechanical behaviour of Lac du Bonnet granite after high-temperature treatment using bonded-particle model and moment tensor. Comput Geosci 135:104132. https://doi.org/10.1016/j.compgeo.2021.104132
Truhar N, Li RC (2021) On an eigenvector-dependent nonlinear eigenvalue problem from the perspective of relative perturbation theory. J Comput Appl Math 395: 113596. https://doi.org/10.1016/j.cam.2021.113596
Ündül Ö, Amann F, Aysal N**,** Plötzec ML (2015) Micro-textural effects on crack initiation and crack propagation of andesitic rocks. Eng Geol 193(2): 267–275. https://doi.org/10.1016/j.enggeo.2015.04.024
Voyiadjis GZ, Kattan PI, Taqieddin ZN (2014) Use of fabric tensors in continuum damage mechanics of solids with micro-cracks. Handb Damage Mech. Springer, New York. https://doi.org/10.1007/978-1-4614-8968-9_3-1
Waqas U, Ahmed MF (2020) Prediction modeling for the estimation of dynamic elastic young's modulus of thermally treated sedimentary rocks using linear–nonlinear regression analysis, regularization, and ANFIS. Rock Mech Rock Eng 53: 5411–5428. https://doi.org/10.1007/s00603-020-02219-8
Wang HL, Chu WJ, He M (2012) Anisotropic permeability evolution model of rock in the process of deformation and failure. J Hydrodynam B 24(1): 25–31. https://doi.org/10.1016/S1001-6058(11)60215-1
Weinan E, Engquist B, Li X, Ren W, Vanden-Eijnden E (2007) Heterogeneous multiscale methods: A review. Comput Phys Commun 2(3): 89–110. https://doi.org/10.1016/j.chaos.2005.08.122
Xia KZ, et al. (2013) Estimation of rock mass mechanical parameters based on ultrasonic velocity of rock mass and Hoek-Brown criterion and its application to engineering. Chin J Rock Mech Eng 32(7): 1458–1466. https://doi.org/10.3969/j.issn.1000-6915.2013.07.022
Zhang, C, Bai, Y (2020) Establishment and application of parametric geometrical damage model of rocks. Rock. Soil. Mech 41(12): 3899–3909. https://doi.org/10.16285/j.rsm.2020.0474
Zhang PF, Zhang YB, Zhao TB, Tan YL, Yu FH (2019) Experimental research on deformation characteristics of waste-rock material in underground backfill mining. Minerals 9(2):102. https://doi.org/10.3390/min9020102
Zhang ZH, Deng JH, Zhu JB, Li LR (2018) An experimental investigation of the failure mechanisms of jointed and intact marble under compression based on quantitative analysis of acoustic emission waveforms. Rock Mech Rock Eng 51(7): 2299–2307. https://doi.org/10.1007/s00603-018-1484-3
Zhang K, Cao P, Meng JJ (2015) Modeling the progressive failure of jointed rock slope using fracture mechanics and the strength reduction method. Rock Mech Rock Eng 48(2): 771–785. https://doi.org/10.1007/s00603-014-0605-x

**Tables**

**Table 1** Comparison of multiscale calculation results

| Method | Input data | | Output data |
|---|---|---|---|
| | Elastic modulus of intact rock, $E$ (GPa) | Initial compressive damage, $D_{t0}$ | Equivalent elastic modulus, $\overline{E}_m$ (GPa) |
| Multiscale calculation approach | 33.8 | 0 | 33.352 |
| | 33.8 | 0.108 | 30.859 |
| | 33.8 | 0.337 | 23.500 |
| Conventional finite element simulation | 33.8 | 0 | 34.574 |
| | 33.8 | 0.108 | 32.163 |
| | 33.8 | 0.337 | 25.716 |
| Laboratory test | 33.8 | 0 | 33.701 |
| | 33.8 | 0.108 | 30.075 |
| | 33.8 | 0.337 | 22.357 |

**Table 2** Multiscale calculation results

| Material | Field uniaxial compressive strength (MPa) | Elastic modulus, $E$ (GPa) | Equivalent elastic modulus, $\overline{E}_m$ (GPa) | Error |
|---|---|---|---|---|
| Rock | 142.48 | 54.46 | — | — |
| ore | 113.52 | 33.7 | — | — |
| pure cement slurry | 4.85 | 3.61 | — | — |
| grouting solidified body | 8.72 | 6.214 | 6.182 (Aggregate: rock) | 0.515% |
| | | | 7.823 (Aggregate: ore) | 25.89% |

**Figures**

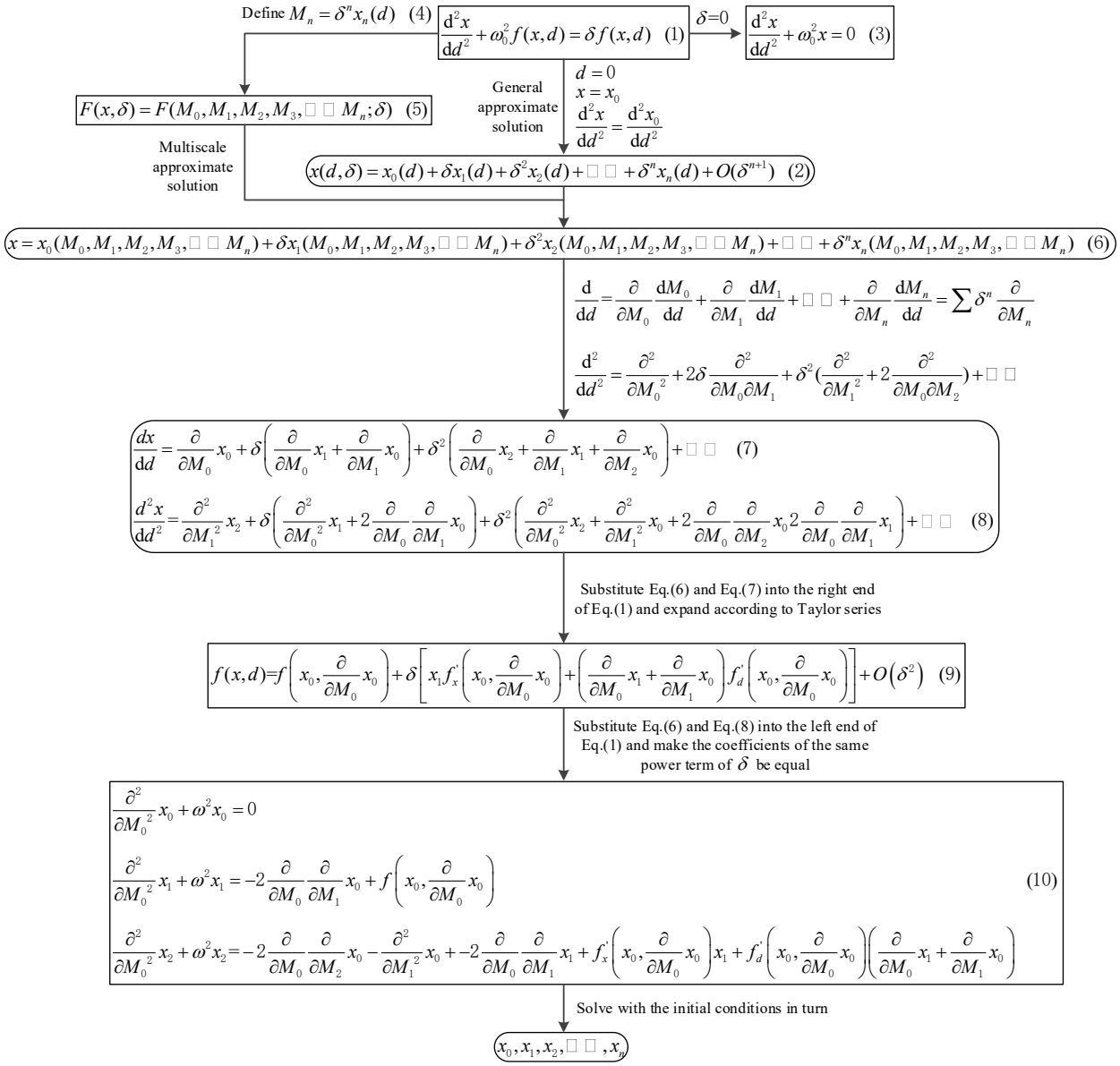


**Fig. 1** General solving procedure for the fundamental perturbation theory (Truhar 2021)

Here, $x$ is the displacement coordinate of the system $S_\delta$, $\delta$ the small parameter of the perturbation equation, and $d$ the physical dimension parameter of $S_\delta$. $\delta f(x,d)$ is a small-scale term, which is regarded as a perturbation term. $\delta$ is independent of the function $x_i(d)$, $i$ = 1, 2, …, and $M_n$ is the solution of the motion equation $\Gamma_\delta$ under the calculation scale $n$, $n$ = 1, 2, 3… $F(x, \delta)$ is a function with multiscale and multiple independent variables.

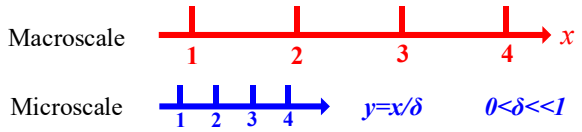


**Fig. 2** Multiscale diagram

Here, $y$ is the microscale displacement coordinate of the rock system, $\delta$ the small parameter of perturbation equation, and $T$ the change cycle of the structural variable field.

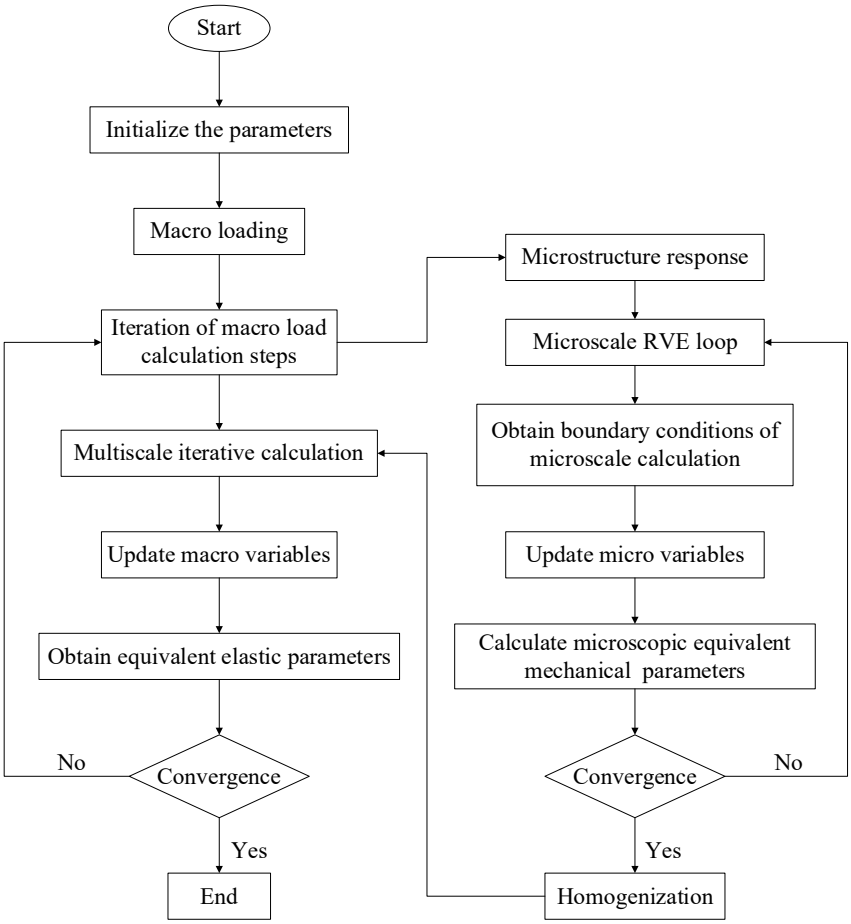


**Fig. 3** Multiscale calculation approach resolve process

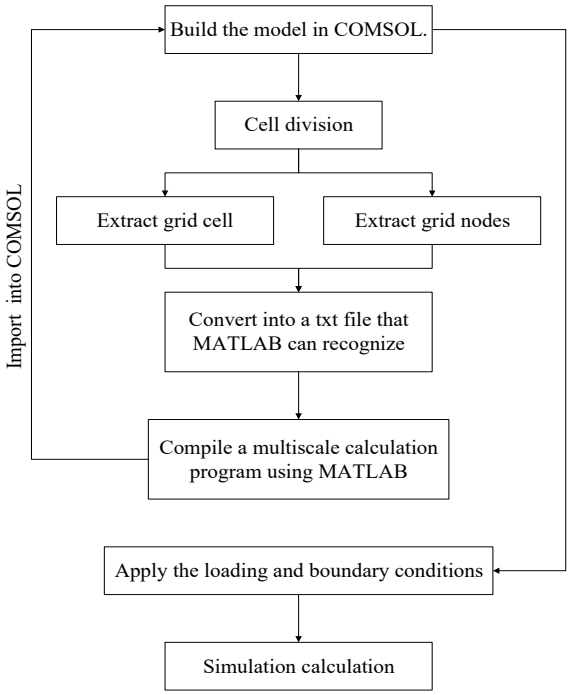


**Fig. 4** Flowchart of the numerical simulation



**Fig. 5** Damaged rock specimens




(a) (b)

**Fig. 6** INSTRON Electro-hydraulic servo universal testing machine: (a) MODEL 1342; (b) MODEL 1346

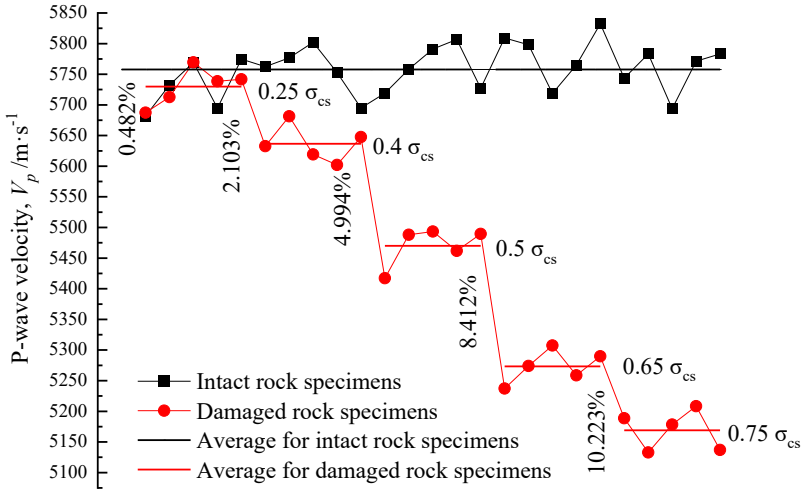


**Fig. 7** P-wave velocity of damaged rock specimens

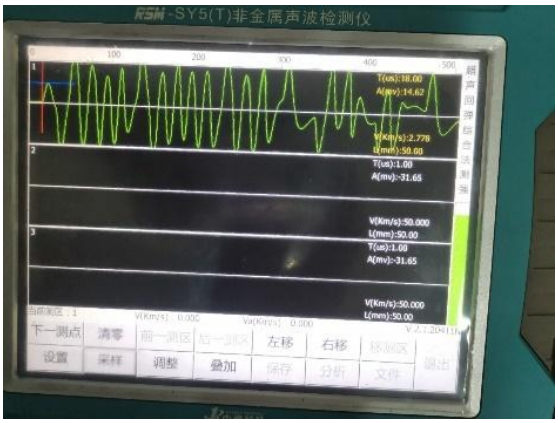


**Fig. 8** RSM-SY5 (T) nonmetallic acoustic wave detector

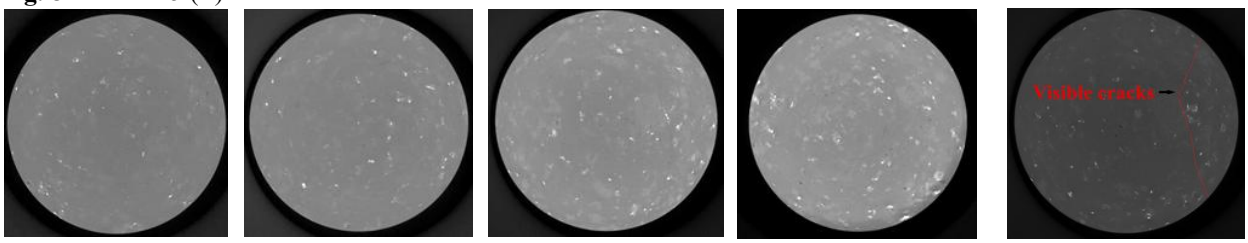


（a） （b） （c） （d） （e）

**Fig. 9** Typical CT scan section of rock specimens with different initial damage: (a) $0.25\sigma_{cs}$; (b) $0.4\sigma_{cs}$; (c) $0.5\sigma_{cs}$; (d) $0.65\sigma_{cs}$; (e) $0.75\sigma_{cs}$

Here, the white areas with a heterogeneous distribution on the CT scan section of rock specimens indicate pores and cracks.




**Fig. 10** AX-3000 industrial micro CT scan system

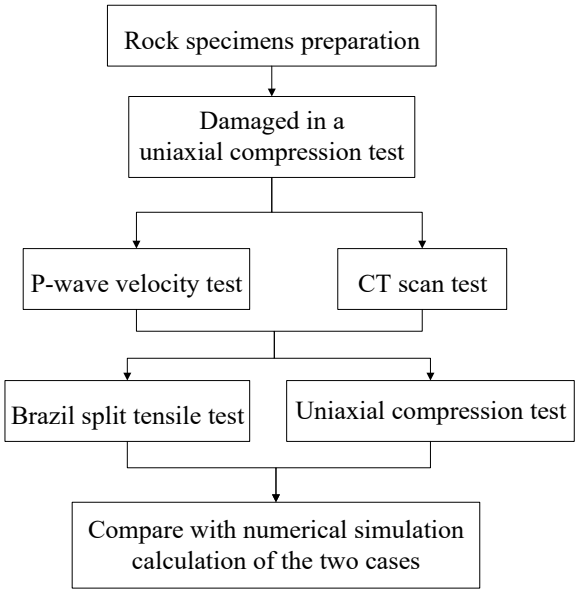


**Fig. 11** Test procedure

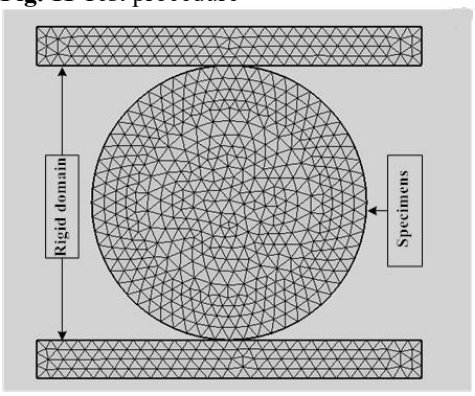


437 **Fig. 12** Schematic of the grid division

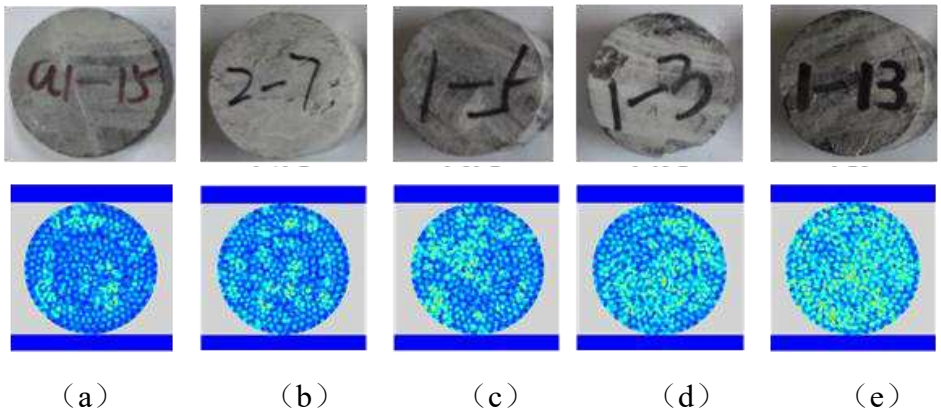


**Fig. 13** Rock specimens and the corresponding numerical models of Brazil split tensile test with different initial damage: (a) $0.25\sigma_{cs}$; (b) $0.4\sigma_{cs}$; (c) $0.5\sigma_{cs}$; (d) $0.65\sigma_{cs}$; (e) $0.75\sigma_{cs}$

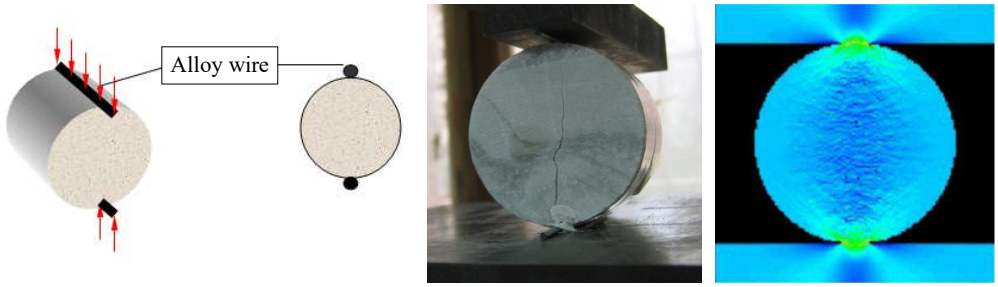


(a) (b) (c)

**Fig. 14** Comparison of test and simulation results: (a) Brazil split tensile test schematic diagram; (b) split specimen after test; (c) numerical model calculation result

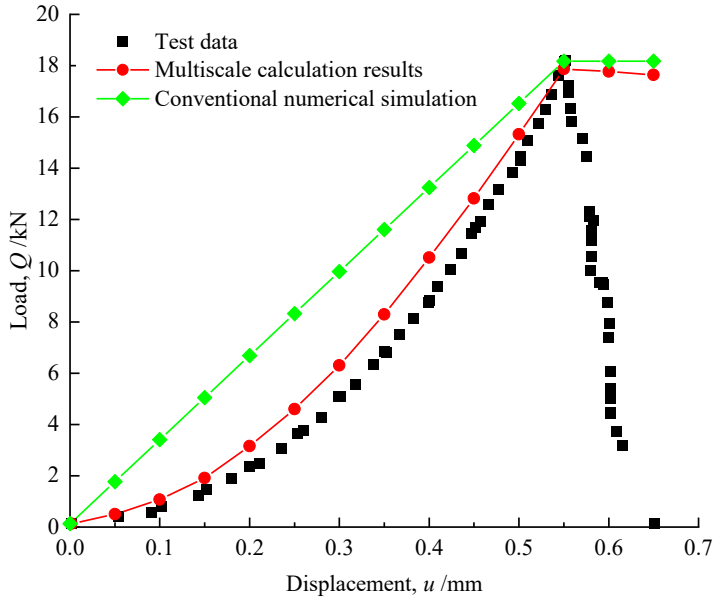


(a)

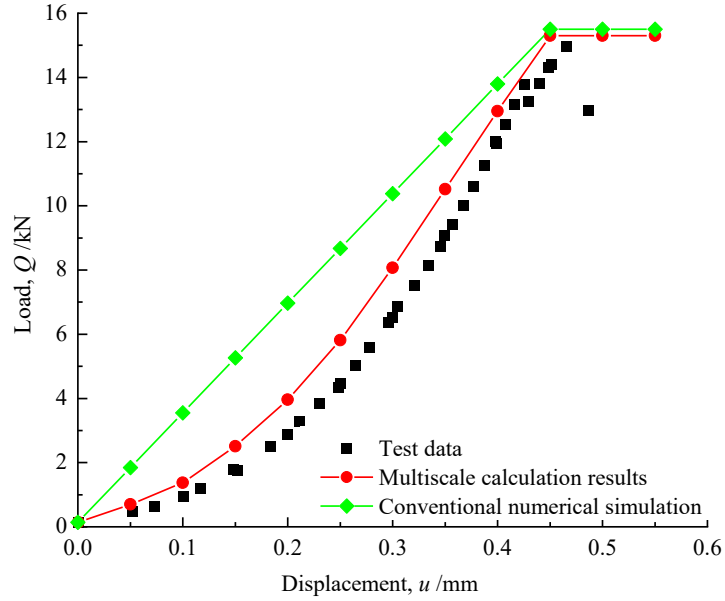


(b)

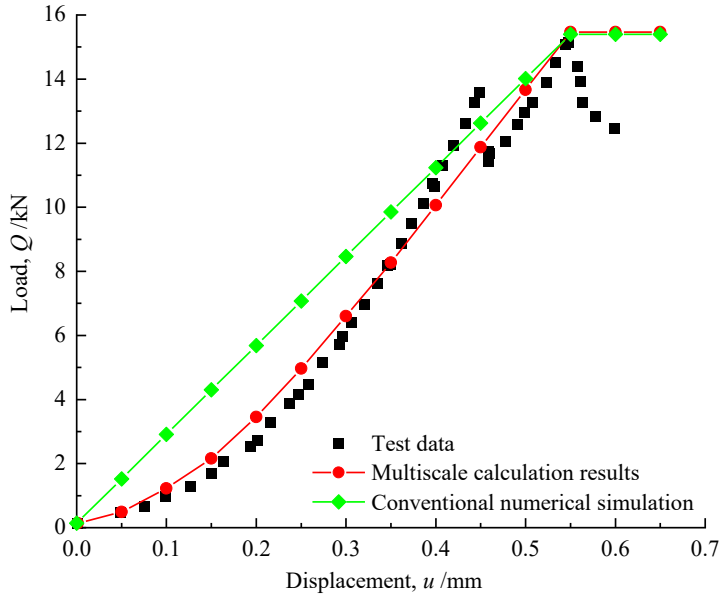
Load, Q /kN
Displacement, u /mm
Test data
Multiscale calculation results
Conventional numerical simulation

(c)

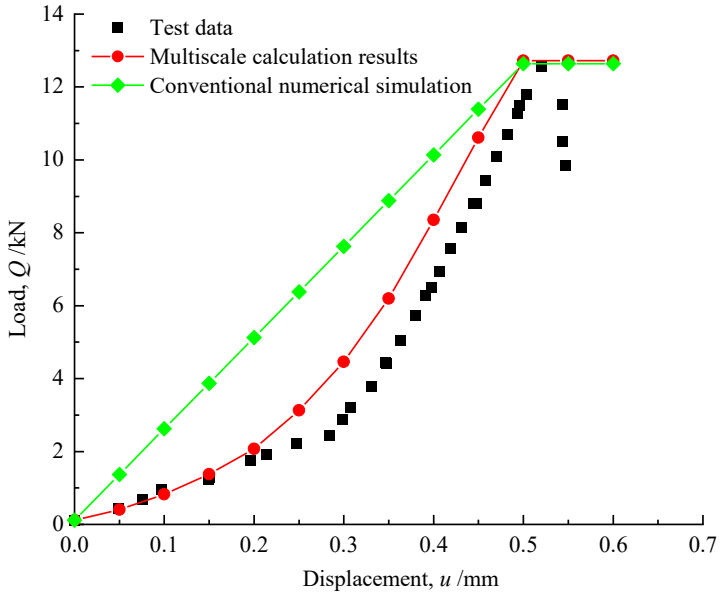
Load, Q /kN
Displacement, u /mm
Test data
Multiscale calculation results
Conventional numerical simulation

(d)

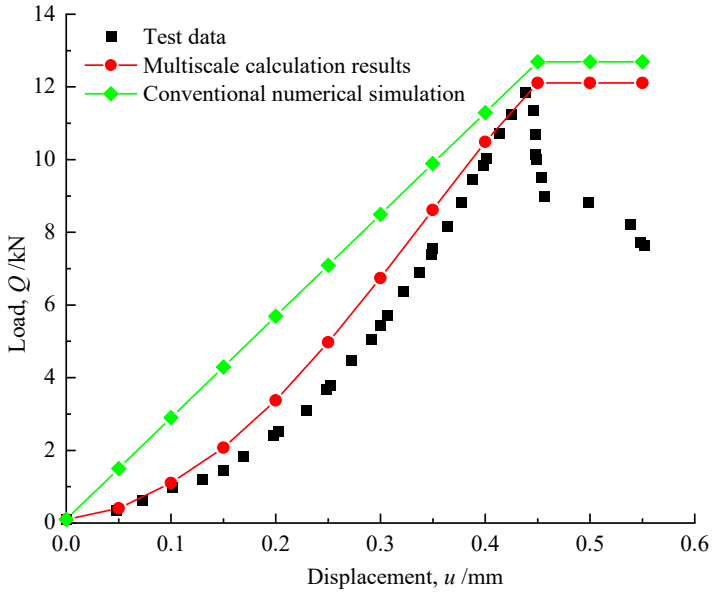


(e)

**Fig. 15** Brazil split tensile load–displacement curves of rock specimens with different initial damage: (a) $0.25\sigma_{cs}$; (b) $0.4\sigma_{cs}$; (c) $0.5\sigma_{cs}$; (d) $0.65\sigma_{cs}$; (e) $0.75\sigma_{cs}$

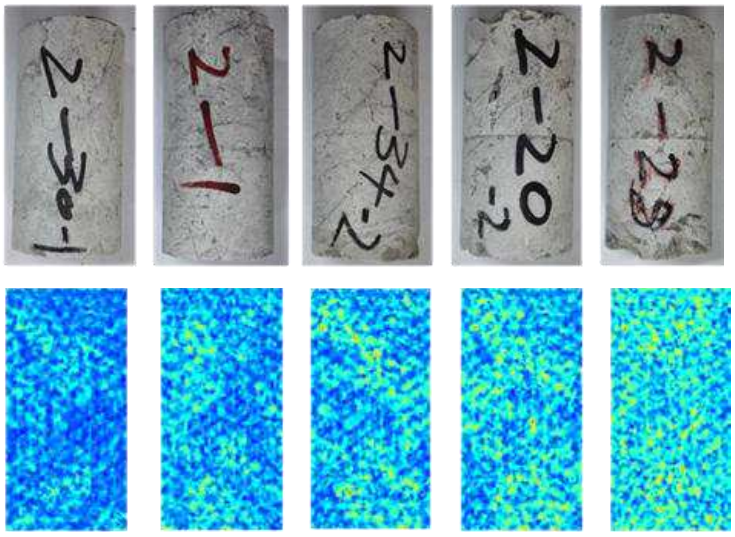

（a） （b） （c） （d） （e）

**Fig. 16** Rock specimens and the corresponding numerical models for uniaxial compression test with different initial damage: (a) $0.25\sigma_{cs}$; (b) $0.4\sigma_{cs}$; (c) $0.5\sigma_{cs}$; (d) $0.65\sigma_{cs}$; (e) $0.75\sigma_{cs}$

438

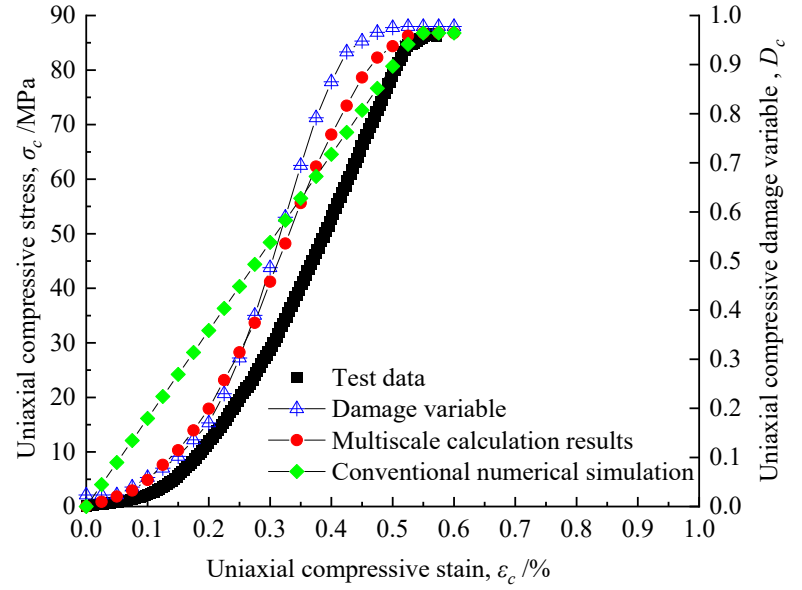
Uniaxial compressive stress, $\sigma_c$ /MPa
Uniaxial compressive damage variable , $D_c$
Uniaxial compressive stain, $\varepsilon_c$ /%
Test data
Damage variable
Multiscale calculation results
Conventional numerical simulation

(a)

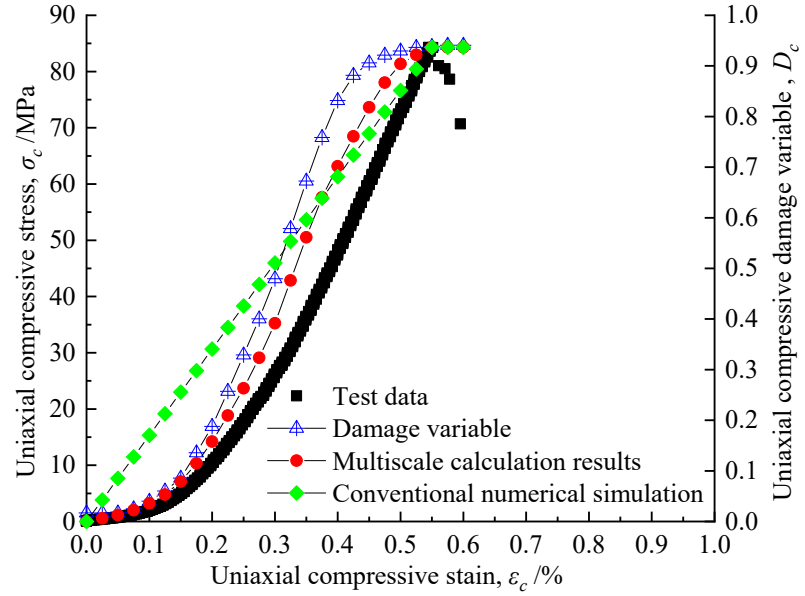
Uniaxial compressive stress, $\sigma_c$ /MPa
Uniaxial compressive damage variable , $D_c$
Uniaxial compressive stain, $\varepsilon_c$ /%
Test data
Damage variable
Multiscale calculation results
Conventional numerical simulation

(b)

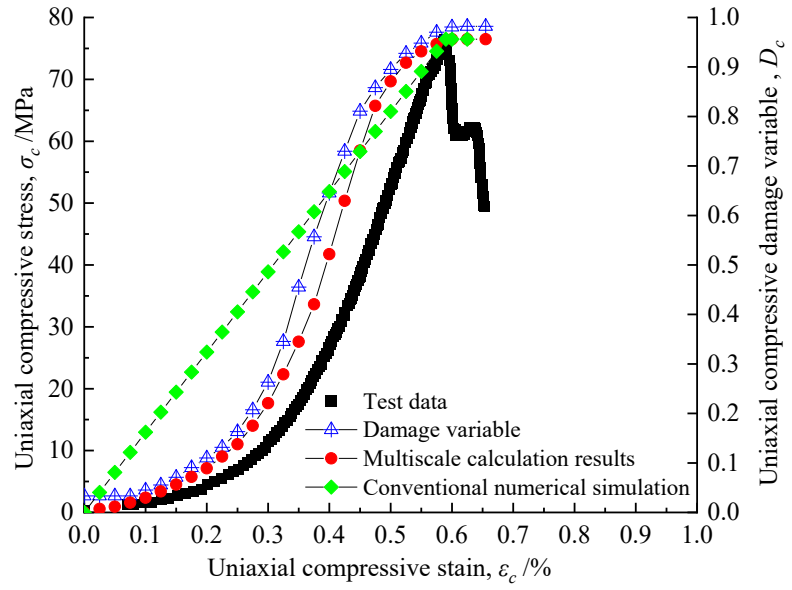
Uniaxial compressive stress, $\sigma_c$ /MPa
Uniaxial compressive damage variable , $D_c$
Uniaxial compressive stain, $\varepsilon_c$ /%
Test data
Damage variable
Multiscale calculation results
Conventional numerical simulation

(c)

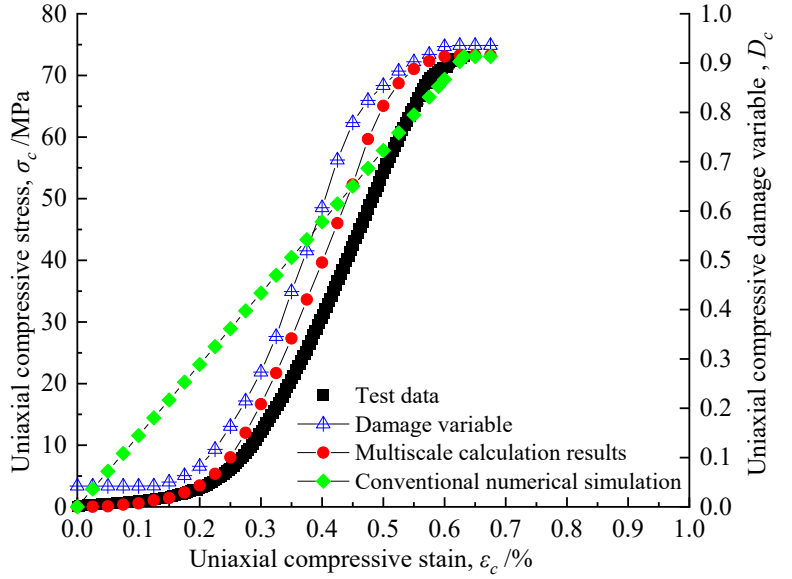
Uniaxial compressive stress, $\sigma_c$ /MPa
Uniaxial compressive damage variable , $D_c$
Uniaxial compressive stain, $\varepsilon_c$ /%
Test data
Damage variable
Multiscale calculation results
Conventional numerical simulation

(d)

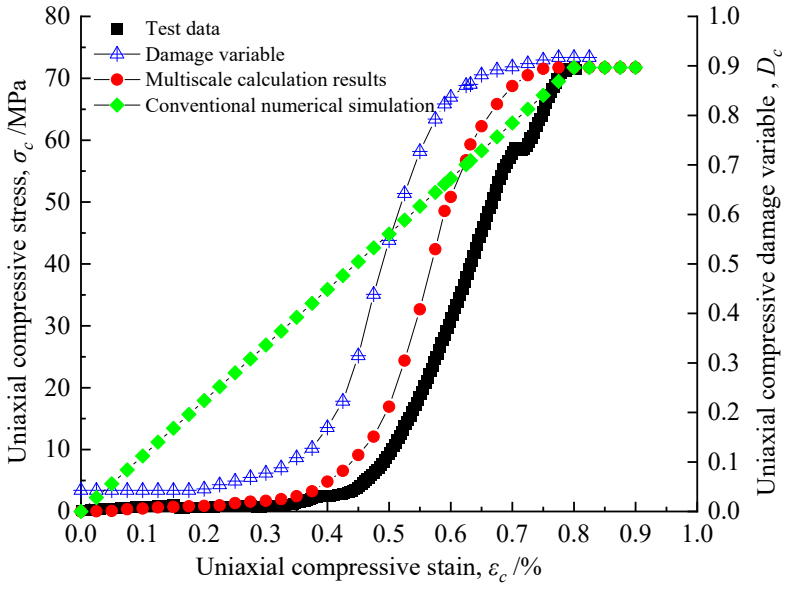


(e)

**Fig. 17** Uniaxial compressive stress–strain curves of rock specimens with different initial damage: (a) $0.25\sigma_{cs}$; (b) $0.4\sigma_{cs}$; (c) $0.5\sigma_{cs}$; (d) $0.65\sigma_{cs}$; (e) $0.75\sigma_{cs}$

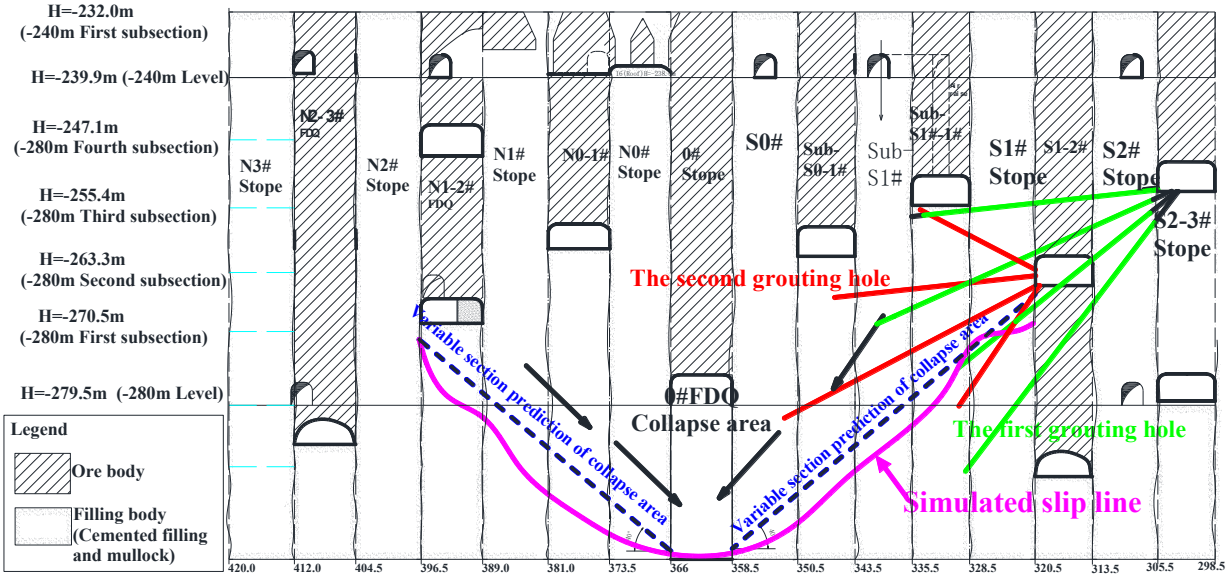


**Fig. 18** Collapsed area in Sh-320 m of the lead–zinc mine

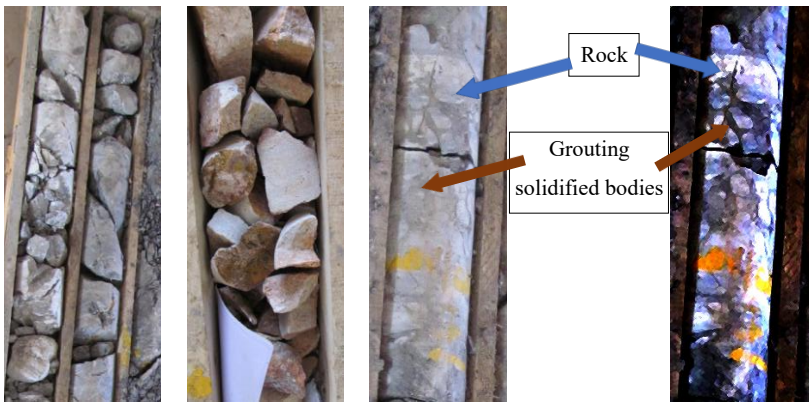


**Fig. 19** Effects of grouting reinforcement: (a) broken rock; (b) rock core; (c) grouting solidified bodies; (d) sharpening effect diagram of grouting solidified bodies

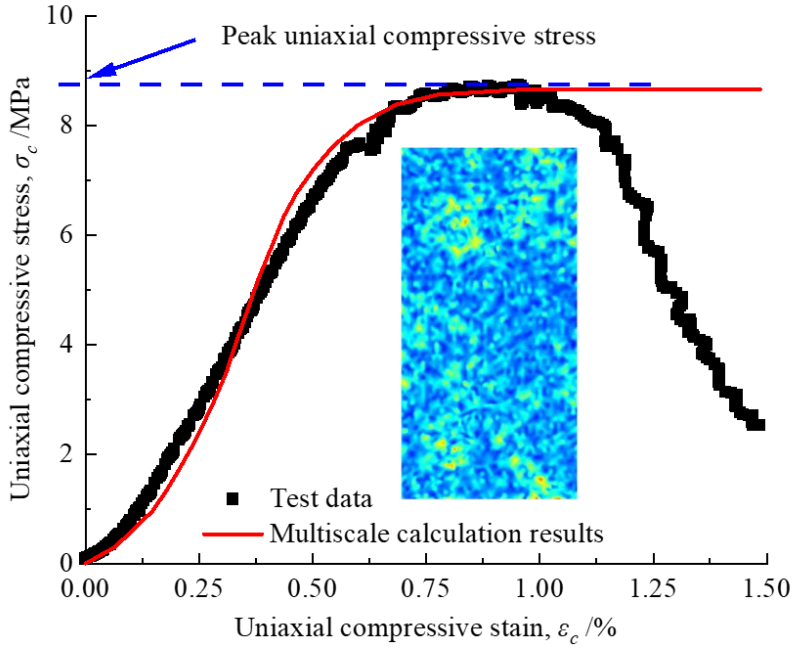


**Fig. 20** Comparison between field compression test and multiscale calculation results